



PERGAMON

Micron 30 (1999) 51–58

---

---

**micron**

---

---

# Cross-sectional scanning tunneling microscopy of mixed-anion semiconductor heterostructures

Edward T. Yu\*

*Department of Electrical and Computer Engineering, University of California at San Diego, La Jolla, CA 92093-0407, USA*

Received 20 January 1998; received in revised form 27 May 1998; accepted 2 June 1998

---

## Abstract

The engineering of advanced heterostructure and nanoscale semiconductor devices has made essential a detailed understanding of, and control over, the structure and properties of semiconductor materials and devices at the atomic to nanometer scale. Cross-sectional scanning tunneling microscopy provides unique and powerful capabilities for characterization of structural morphology and electronic properties in semiconductor epitaxial and device structures with spatial resolution at or near the atomic scale. The basic technique of cross-sectional scanning tunneling microscopy, and key experimental considerations, are described in this article. Some representative applications of this technique drawn from recent investigations in our laboratory of atomic-scale alloy layer and interface structure in mixed-anion semiconductor heterostructures are presented. By combining the results of scanning tunneling microscopy studies with those of other, complementary characterization techniques, it is possible to develop a detailed understanding of atomic- to nanometer-scale properties of semiconductor materials and devices and to establish correlations between atomic-scale material properties and the behavior of actual devices. © 1999 Elsevier Science Ltd. All rights reserved.

*Keywords:* Scanning tunneling microscopy; Semiconductor; Heterostructure; Heterojunction; III–V; Cross-sectional; Atomic; Nanometer

---

## 1. Introduction

Since its invention in the early 1980s, scanning tunneling microscopy (STM) and other scanning probe techniques such as atomic force microscopy (AFM) that evolved from it have become tools of paramount importance in fundamental studies of metal and semiconductor surfaces. In addition, increasing effort has been directed towards the application of STM and related techniques to address problems of technological interest; a substantial part of this effort has been devoted to nanoscale characterization of semiconductor materials and devices.

As the characteristic dimensions of semiconductor devices continue to shrink and as advanced semiconductor heterostructure devices increase in prominence, the ability to characterize structure and electronic properties in semiconductor materials and device structures with atomic to nanometer-scale spatial resolution has assumed dramatically increased importance. Phenomena such as atomic-scale roughness of semiconductor heterojunction interfaces (Tanaka et al., 1992; Förster et al., 1993; Hoffman et al., 1993), compositional ordering and clustering within

semiconductor alloys (Stringfellow and Chen, 1991), discreteness and spatial distribution of dopant atoms, and self-assembly of nanoscale structures (Bimberg et al., 1998) can exert a pronounced influence on material properties and device behavior. The rapidly increasing importance of STM and other scanning probe techniques in semiconductor science and technology is a natural consequence of the desire to design and fabricate ever smaller structures to improve device performance or achieve new device functionality, and of the limitations of more traditional experimental techniques in performing detailed and comprehensive characterization at the atomic to nanometer scale.

In this article, we discuss the basic experimental considerations and techniques involved in cross-sectional STM, and describe some representative applications of this technique drawn from our recent investigations of atomic-scale alloy layer and interface structure in mixed-anion semiconductor heterostructures. Cross-sectional STM has emerged as a unique and powerful tool in the study of atomic-scale properties in III–V compound semiconductor heterostructures, and also in the study of nanometer-scale structure and electronic properties in Si microelectronic devices, offering unique capabilities for characterization that, in conjunction with other, complementary experimental techniques provide new and important insights into material and device

---

\* Tel.: +1 619 5346619; fax: +1 619 5340556.

E-mail address: [ety@ece.ucsd.edu](mailto:ety@ece.ucsd.edu) (E.T. Yu)

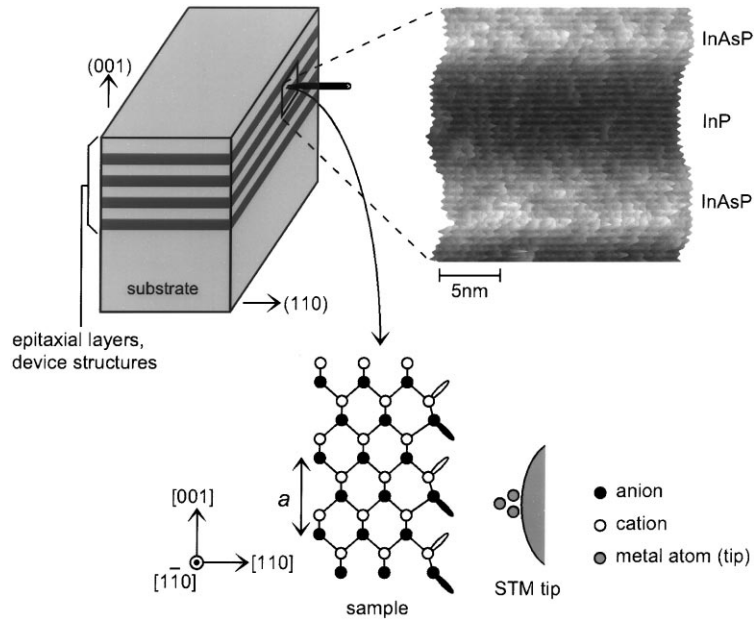


Fig. 1. Schematic diagram of the sample and probe-tip geometry and of the arrangement of atoms in the sample and tip, and a representative image in cross-sectional scanning tunneling microscopy. Typically an (001) semiconductor wafer is cleaved to expose a (110) cross-sectional surface. Tunneling measurements are then performed with the probe tip positioned over the region of interest – generally consisting of epitaxial layers grown or device structures fabricated on the surface of the wafer – on the cross-sectional surface. The image shown is of an InP/InAs<sub>0.35</sub>P<sub>0.65</sub> heterostructure.

properties at the atomic to nanometer scale (Murali and Pohl, 1986; Salemink et al., 1989; Smith et al., 1994; Zheng et al., 1994; Feenstra et al., 1994; Lew et al., 1994; Skala et al., 1995). The unique and powerful advantage offered by STM and other scanning probe techniques is the ability to perform direct studies of structural, electronic, and other properties of materials with extremely high spatial resolution. Many other techniques, such as X-ray diffraction, electron diffraction, and transmission electron microscopy, typically provide less direct information about sample structure and, while offering the ability to probe certain structural or compositional features at the atomic scale, inevitably average these properties over larger areas or volumes. In STM, direct imaging of features corresponding to individual atoms on a surface has been demonstrated for a wide range of materials. Other scanning probe techniques, while typically providing somewhat lower spatial resolution than STM, allow greater flexibility in samples that can be studied, imaging conditions that can be tolerated, and properties that can be characterized. Rapid progress in the development of new scanning probe techniques and in the commercial availability of scanning probe instrumentation has led to the widespread application of these techniques to problems of both scientific and technological importance.

## 2. Experimental technique

In cross-sectional STM, a semiconductor wafer is cleaved to expose a cross section – typically a (110) or (111)

plane – of epitaxial layers grown or device structures fabricated on the wafer. Tunneling measurements performed on the exposed cross-sectional surface can then reveal information about the atomic-scale morphology and electronic structure of these epitaxial layers or devices. Fig. 1 shows the typical geometry of the sample and STM probe tip in cross-sectional STM; a schematic illustration of the atomic structure of the sample and probe tip near the (110) cleaved surface of a zinc-blende semiconductor; and a representative, atomically resolved cross-sectional STM image of an InP/InAs<sub>x</sub>P<sub>1-x</sub> heterostructure obtained in our laboratory.

As indicated schematically in Fig. 1, the cation and anion sites in the {110} surface plane of a compound semiconductor contain empty and filled dangling-bond states, respectively. STM imaging of the GaAs (110) surface has shown that for positive bias voltage applied to the sample, one obtains images of the unoccupied orbitals corresponding to the Ga (cation) sites on the (110) surface, while for negative sample bias the As (anion) sublattice on the (110) surface is imaged (Feenstra et al., 1987). Detailed STM studies of the GaAs (110) surface have shown that only a mild surface reconstruction occurs, consisting of some buckling and bond reorientation within a (1 × 1) unit cell. For Group-IV elemental semiconductors, obtaining atomically flat cross-sectional surfaces is somewhat problematic: the as-cleaved (110) surface was found to be disordered (Lutz et al., 1995), with complex surface reconstructions appearing upon annealing at high temperature (Van Loenen et al., 1988; Dijkamp et al., 1990). However, hydrogen passivation of the (110) surface can be accomplished by dipping a Si wafer cleaved ex situ in

hydrofluoric acid (Johnson and Halbout, 1992), or by exposure of a clean, in situ cleaved (1 1 0) surface to atomic hydrogen in vacuo (Lutz et al., 1995). Such a procedure is required to obtain a (1 1 0) surface that is not strongly pinned, i.e., a surface for which the density of surface states associated with defects or contamination is sufficiently low, such that the electronic properties of the bulk material can be probed via tunneling measurements.

### 3. III–V semiconductor characterization

A broad range of advanced heterostructure device concepts has been developed and explored in III–V semiconductor material systems; for almost all such devices, the atomic- to nanometer-scale structure of the constituent alloy layers and heterojunction interfaces exerts a significant influence on device performance: for example, atomic-scale interface roughness can influence transport properties in heterojunction field-effect transistors and spectral response in quantum-well-based optoelectronic devices; clustering and ordering within alloy layers can produce substantial changes in the band gap of an alloy; and interface stoichiometry can be a major factor in determining optical, electronic, and transport properties in mixed-anion heterojunction material systems. A detailed understanding of these phenomena and their relationship to epitaxial crystal growth conditions and to device behavior plays an essential role in the development and optimization of advanced heterostructure devices; cross-sectional STM can contribute in unique and powerful ways to the development of this understanding.

III–V semiconductors are in many respects ideally suited for study by cross-sectional STM. Cleaving of (0 0 1) wafers can produce (1 1 0) cross-sectional surfaces with atomically flat planes extending over tens to hundreds of nanometers. To avoid contamination of the cleaved surface, cleaving must be performed under ultrahigh-vacuum conditions. Furthermore, for atomically flat (1 1 0) surfaces of most III–V semiconductors, the Fermi level at the surface is unpinned; consequently, tunneling spectroscopy performed on the cleaved (1 1 0) surface can yield information about the bulk, as opposed to purely surface-related, electronic properties of the material.

In constant-current cross-sectional images of heterostructures, apparent “topographic” contrast between the different materials present in the heterostructure is typically observed, with corrugation amplitudes ranging from less than 0.1 nm to over 10 nm. This contrast is generally ascribed to differences in the electronic properties of the constituent materials, rather than to actual physical topography on the cross-sectional surface. Factors such as differing energy band gaps, dopant and carrier concentrations, and electron affinities can contribute to the apparent topographic contrast between materials in a heterostructure, with variations in band-edge energy from one layer to the next

generally being the dominant contributing factor to the observed heterostructure contrast.

As STM imaging is sensitive primarily to the one or two uppermost layers on the surface of the sample, atomic-scale features in structure and electronic properties can be resolved with considerably greater detail in cross-sectional STM than in other techniques. High-resolution X-ray diffraction can in some circumstances yield information about atomic-scale interface structure in superlattices, but this information is generally averaged over many layers and also over a large area of the sample. Transmission electron microscopy can provide information about atomic-scale interface structure, but averaging that occurs through the thickness of the sample – typically of the order of 10 nm or more – limits the technique’s ability to resolve features such as atomic-scale interface roughness and fluctuations in composition.

Atomically resolved STM imaging of cross-sectional surfaces of epitaxial layers, which so far has been achieved only for III–V semiconductors and under ultrahigh-vacuum conditions, is therefore a uniquely powerful tool for exploring alloy layer and heterojunction interface structure at the atomic scale. By combining information obtained from cross-sectional STM with results obtained using complementary characterization techniques such as X-ray diffraction, electron diffraction, electron microscopy, and electrical and optical measurements, it is possible to develop a detailed understanding of atomic- to nanometer-scale properties of semiconductor materials and devices, confirm that this information is representative of properties at the larger length scales relevant for most device structures, and ultimately establish correlations between atomic-scale material properties and the behavior of actual devices.

## 4. Characterization of mixed-anion heterostructures

### 4.1. *InAs/Ga<sub>1-x</sub>In<sub>x</sub>Sb*

Mixed-anion material systems, in which the Group V as well as the Group III constituent changes across a heterojunction interface, are particularly rich in possibilities for complex interfacial structure. In these material systems, two distinct bond configurations, both of which correspond to a “structurally perfect” heterojunction, can be present at each interface (Tuttle et al., 1990). Furthermore, it has been demonstrated that interfacial composition can exert considerable influence on electron transport (Tuttle et al., 1990), optical properties (Brar et al., 1994), and electronic structure (Chow et al., 1992), particularly in arsenide/antimonide heterojunctions. Cross-sectional STM studies of such structures have begun to provide insight into the atomic-scale structure of heterojunction interfaces and alloy layers in these material systems (Feenstra et al., 1994; Lew et al., 1994).

Of particular importance for studies in which the

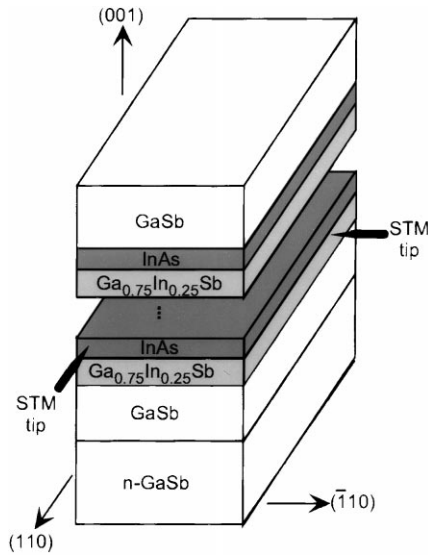


Fig. 2. Schematic diagram of the InAs/Ga<sub>0.75</sub>In<sub>0.25</sub>Sb superlattice structure and of the probe tip geometry for (1 1 0) and ( $\bar{1}$  1 0) cross-sectional tunneling measurements.

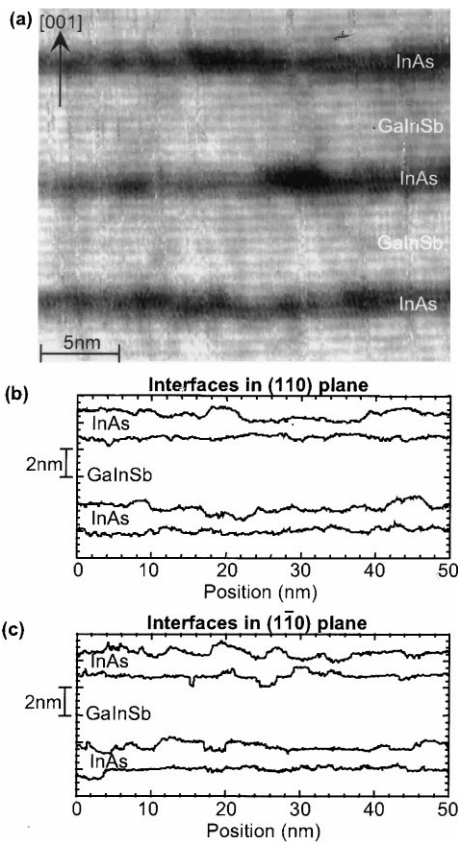


Fig. 3. (a) Filled-state, constant-current (1 1 0) cross-sectional image of the InAs/Ga<sub>0.75</sub>In<sub>0.25</sub>Sb superlattice; (b) heterojunction interface profiles extracted from (1 1 0) cross-sectional STM images; (c) interface profiles extracted from (1  $\bar{1}$  0) images.

correlation between atomic-scale alloy layer and interface structure and device behavior is of primary interest is the ability to quantify properties such as interface roughness. Cross-sectional STM provides a highly effective means of obtaining such information, with quantitative studies of interface roughness in InAs/GaSb superlattices (Feenstra et al., 1994) and InP/InGaAs resonant-tunneling-diode structures (Skala et al., 1995) having been performed. As an illustration of the quantitative analysis of interface roughness using STM, we describe briefly our studies of the dependence of interface roughness in InAs/Ga<sub>1-x</sub>In<sub>x</sub>Sb superlattices on orientation and growth sequence (Lew et al., 1997; Lew et al., 1998). The sample structure and experimental geometry employed in these studies are shown in Fig. 2. As indicated in the figure, STM imaging of both the (1 1 0) and ( $\bar{1}$  1 0) cross-sectional surfaces was performed, allowing the dependence of interface structure on both orientation and growth sequence to be investigated. Fig. 3(a) shows a cross-sectional STM image, obtained at a sample bias of  $-1.5$  V and tunneling current of 0.1 nA, of a 17 Å InAs/50 Å Ga<sub>0.75</sub>In<sub>0.25</sub>Sb superlattice grown on a GaSb (0 0 1) substrate. Interfaces between the InAs (dark) and Ga<sub>0.75</sub>In<sub>0.25</sub>Sb (bright) layers can be extracted from images of both (1 1 0) and (1  $\bar{1}$  0) cross-sectional surfaces using an edge-detection algorithm to identify the interfaces. Figs. 3(b) and (c) show representative interfaces extracted from images of the (1 1 0) and (1  $\bar{1}$  0) cross-sectional surfaces, respectively. Analysis of images in this manner allows detailed, quantitative information about interface structure and its dependence on orientation and growth sequence to be obtained.

Interface roughness can then be quantified by performing a Fourier analysis of the interface profiles extracted as described above. The power spectral distribution for interface profiles extracted from our STM images was found to be well described by a Lorentzian function,

$$|A_q|^2 = \frac{1}{L} \frac{2\Delta^2(\Lambda/2\pi)}{1 + (q\Lambda/2\pi)^2}, \quad (1)$$

where  $\Delta$  is the roughness amplitude,  $\Lambda$  the correlation length, and  $L$  the length of each interface profile in real space. Separate power spectral distributions were calculated for InAs-on-Ga<sub>0.75</sub>In<sub>0.25</sub>Sb and Ga<sub>0.75</sub>In<sub>0.25</sub>Sb-on-InAs interfaces, and for interfaces in the (1 1 0) and (1  $\bar{1}$  0) cross-sectional planes, with the roughness parameters obtained shown in Table 1. Two significant conclusions may be drawn from this analysis: first, interfaces imaged in the (1  $\bar{1}$  0) cross-sectional plane are rougher than those in the (1 1 0) plane; and second, there exists a substantial dependence of interface roughness on growth sequence – for imaging in both the (1 1 0) and (1  $\bar{1}$  0) planes, interfaces in which Ga<sub>0.75</sub>In<sub>0.25</sub>Sb was grown on InAs were found to be significantly rougher than those in which InAs was grown on Ga<sub>0.75</sub>In<sub>0.25</sub>Sb.

The observation of anisotropy in interface roughness can

Table 1  
Roughness amplitudes and correlation lengths for various types of interfaces in the InAs/Ga<sub>0.75</sub>In<sub>0.25</sub>Sb superlattice

Cross-sectional plane	Interface	Amplitude $\Delta$ (Å)	Correlation length $\Lambda$ (Å)
(1 $\bar{1}$ 0)	Ga <sub>0.75</sub> In <sub>0.25</sub> Sb-on-InAs	4.3 ± 0.2	327 ± 38
(1 $\bar{1}$ 0)	InAs-on-Ga <sub>0.75</sub> In <sub>0.25</sub> Sb	2.8 ± 0.2	174 ± 21
(1 1 0)	Ga <sub>0.75</sub> In <sub>0.25</sub> Sb-on-InAs	3.2 ± 0.2	301 ± 39
(1 1 0)	InAs-on-Ga <sub>0.75</sub> In <sub>0.25</sub> Sb	1.9 ± 0.1	112 ± 16

be explained by previously reported observations that, for MBE-grown surfaces of a variety of III–V semiconductors, islands and terraces are formed that are elongated preferentially along the [1  $\bar{1}$  0] direction (Pashley et al., 1991; Sudijono et al., 1992; Heller and Lagally, 1992; Thibado et al., 1995). For two-dimensional growth, such features on the surface would be expected to produce corresponding features in epitaxially grown interfaces. Cross-sections of such interfaces would then exhibit greater roughness along the [1 1 0] direction, i.e., in the (1  $\bar{1}$  0) plane, than along the [1  $\bar{1}$  0] direction – precisely as is found in our STM studies.

The dependence of interface roughness on growth sequence is consistent with the formation of interfaces with mixed stoichiometry for Ga<sub>0.75</sub>In<sub>0.25</sub>Sb grown on InAs and of stoichiometrically uniform interfaces for InAs grown on Ga<sub>0.75</sub>In<sub>0.25</sub>Sb. Previous studies had indicated that for InAs/Ga<sub>1-x</sub>In<sub>x</sub>Sb infrared detectors, device characteristics may be optimized by deliberate growth of structures in which InSb-like composition is present at each heterojunction interface (Miles et al., 1993). In the growth of InAs/Ga<sub>0.75</sub>In<sub>0.25</sub>Sb superlattices by MBE, however, obtaining

InSb-like composition at the Ga<sub>0.75</sub>In<sub>0.25</sub>Sb-on-InAs interface requires that the As layer present on the InAs surface be replaced by a layer of Sb prior to initiating deposition of Ga<sub>0.75</sub>In<sub>0.25</sub>Sb. While studies by reflection high-energy electron diffraction and X-ray photoelectron spectroscopy indicate that substantial substitution of Sb for As can be achieved by exposure of the As-terminated InAs surface to a pure Sb flux (Wang et al., 1993; Collins et al., 1994), X-ray diffraction studies indicate that only partial substitution of Sb for As occurs under typical growth conditions (Miles et al., 1992). As shown in Fig. 4, the presence of mixed stoichiometry at a Ga<sub>0.75</sub>In<sub>0.25</sub>Sb/InAs interface will lead to interfacial roughness in excess of that present at an interface with uniform stoichiometry. Again, this is precisely as observed in our STM studies.

A semiquantitative correlation between these STM studies and transport behavior in a device structure has also been observed (Lew et al., 1998). Previous studies of InAs/Ga<sub>0.75</sub>In<sub>0.25</sub>Sb superlattices have shown that, at low temperature, lateral carrier mobility is dominated by interface roughness scattering (Hoffman et al., 1993; Hoffman et al., 1994). Measurements of Hall mobility in the [1 1 0] and [1  $\bar{1}$  0] directions in the same superlattice sample as that used in our STM studies have shown that, at low temperature, a substantial anisotropy in mobility exists: the mobility in the [1  $\bar{1}$  0] direction is typically a factor of approximately two higher than that in the [1 1 0] direction. An estimate of interface roughness scattering times may be made using the relation (Goodnick et al., 1985)

$$\frac{1}{\tau(k)} = \frac{e^2 F_s^2 m^*}{2\pi\hbar^3} \int_0^{2\pi} d\theta (1 - \cos \theta) S(q) \times \left[ \frac{\Gamma(q)}{\varepsilon(q)} \right]^2, \quad (2)$$

$$q = 2k \sin \theta/2,$$

where  $F_s$  is the average surface field,  $m^*$  is the effective mass parallel to the interface,  $k$  is the electron wave vector,  $\theta$  is the scattering angle,  $\Gamma(q)$  contains corrections for the image potential and electric field modification at the deformed interface, and  $\varepsilon(q)$  is the electron dielectric function.  $S(q)$  is the matrix element for interface roughness scattering, given by the Fourier transform of the distribution of steps at each interface or, equivalently, by the Fourier transform of the autocorrelation of the interface profiles, which is given by Eq. (1). The drift mobility is related directly to the scattering times by the equation  $\mu = e\langle\tau\rangle/m^*$ . Assuming a Hall scattering factor of unity, we can calculate the ratio of scattering times, and therefore of the Hall mobilities, in the

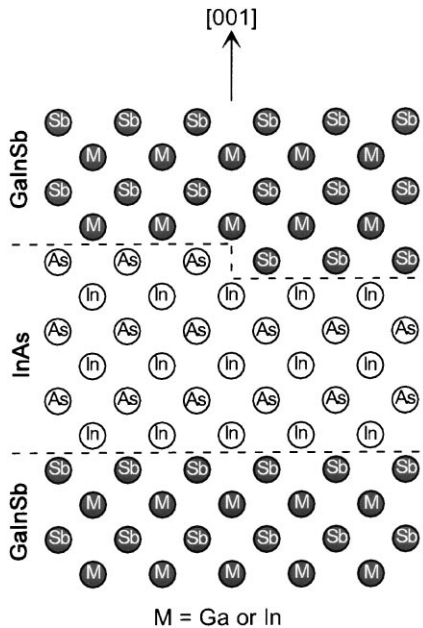


Fig. 4. Schematic diagram of the arrangement of atoms in an InAs/GaInSb superlattice in which uniform, InSb-like stoichiometry is present at the InAs-on-GaInSb interface and mixed stoichiometry is present at the GaInSb-on-InAs interface. Mixed stoichiometry at the upper interface leads to additional atomic-scale roughness at that interface.

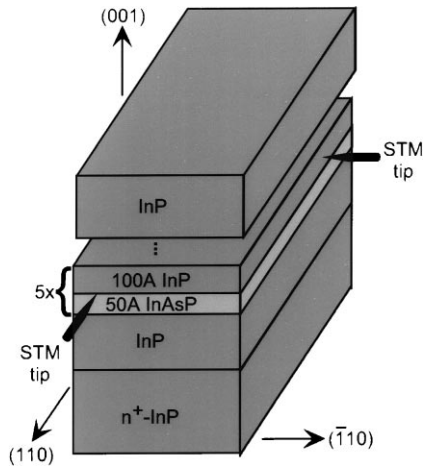


Fig. 5. Schematic diagram of the InP/InAs<sub>0.35</sub>P<sub>0.65</sub> multiple-quantum-well structure and of the probe tip geometry for (110) and  $(\bar{1}10)$  cross-sectional tunneling measurements.

$[110]$  and  $[1\bar{1}0]$  directions. Such an analysis yields a wave-vector-dependent mobility anisotropy ranging from 1.6 to 2.3, in reasonably good quantitative agreement with the mobility anisotropy measured directly in low-temperature transport studies. These studies have provided unique insight into, and demonstrated the power of cross-sectional STM in elucidating, atomic-scale morphology in heterostructures and its relation to growth conditions and device behavior.

#### 4.2. InP/InAs<sub>x</sub>P<sub>1-x</sub>

InP/InAs<sub>x</sub>P<sub>1-x</sub> heterostructures are emerging as promising materials for optoelectronic devices such as lasers and photodetectors operating at 1.06–1.55  $\mu\text{m}$  and for high-speed electronic devices (Woodward and Chiu, 1992; Hou et al., 1993; Kim et al., 1995). A very significant issue for

InAs<sub>x</sub>P<sub>1-x</sub> and many other ternary and quaternary III–V alloys is the possible presence of ordering, clustering, and/or compositional modulation, phenomena that have been observed to occur in a wide range of material systems (Ihm et al., 1987; Jen et al., 1989a; Jen et al., 1989b), and that can exert a considerable influence on crystal quality, interface quality, and other electronic as well as optical properties such as band gap, band-edge discontinuities, and carrier transport (Bhattacharya and Ku, 1985; Gomyo and Suzuki, 1988; Stringfellow and Chen, 1991; Mäder and Zunger, 1994). Detailed characterization and understanding of these phenomena at the atomic scale are therefore of great importance for optoelectronic and electronic devices based on these materials.

Cross-sectional STM studies of InP/InAs<sub>x</sub>P<sub>1-x</sub> heterostructures have provided insight into the nanoscale compositional structure of InAs<sub>x</sub>P<sub>1-x</sub> alloys and InP/InAs<sub>x</sub>P<sub>1-x</sub> heterojunction interfaces grown by gas-source MBE. The sample structure and cross-sectional STM geometry used in these studies are shown in Fig. 5. Fig. 6 shows a three-dimensional rendering of a  $20 \times 20 \text{ nm}^2$  constant-current image of the InP/InAs<sub>0.35</sub>P<sub>0.65</sub> multiple-quantum-well structure obtained from a  $(110)$  cross-sectional plane at a sample bias of  $-2.4 \text{ V}$  and a tunneling current of  $0.1 \text{ nA}$ . As the valence-band edge of InAs has a higher energy than that of InP, we interpret the brighter features as being associated with As orbitals, and the darker features with P orbitals within the InAs<sub>0.35</sub>P<sub>0.65</sub> layer. An asymmetry in interfacial abruptness is apparent, with the InAs<sub>0.35</sub>P<sub>0.65</sub>-on-InP interface appearing to be relatively abrupt, while the InP-on-InAs<sub>0.35</sub>P<sub>0.65</sub> interface exhibits greater roughness and compositional grading. In addition, variations in composition at the atomic to nanometer scale are clearly visible, allowing us to investigate in detail the nature and degree of clustering present in the alloy.

Nanoscale As-rich (bright) and P-rich (dark) clusters are

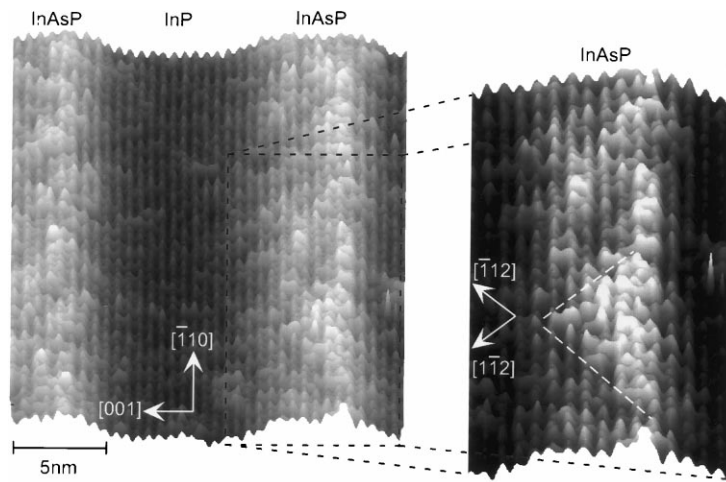


Fig. 6.  $(110)$  cross-sectional image of the InP/InAs<sub>0.35</sub>P<sub>0.65</sub> multiple-quantum-well structure, obtained at a sample bias of  $-2.4 \text{ V}$  and a tunneling current of  $0.1 \text{ nA}$ . Significant compositional variation at the nanometer scale is visible in the large-area image. In the magnified view of the InAs<sub>0.35</sub>P<sub>0.65</sub> alloy layer, the detailed structure of an As-rich cluster is visible, showing the presence of boundaries oriented along  $\{112\}$  directions within the  $(110)$  cross-sectional plane.

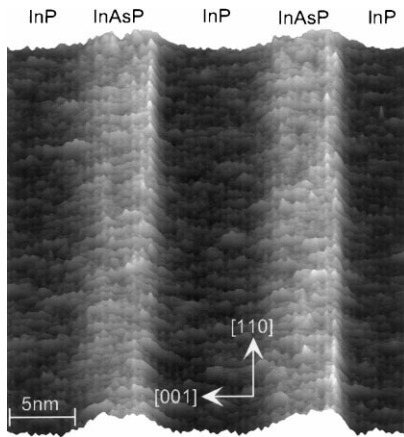


Fig. 7.  $(1\bar{1}0)$  cross-sectional image of the InP/InAs<sub>0.35</sub>P<sub>0.65</sub> multiple-quantum-well structure, obtained at a sample bias of  $-2.4$  V and a tunneling current of  $0.1$  nA. Nanoscale lateral variations in composition within the InAs<sub>0.35</sub>P<sub>0.65</sub> alloy are less apparent than in the  $(110)$  cross-sectional image, suggesting the formation of As-rich clusters elongated along the  $[1\bar{1}0]$  direction within the alloy.

clearly seen within the InAs<sub>0.35</sub>P<sub>0.65</sub> layer in Fig. 6. The figure also shows a magnified view of the InAs<sub>0.35</sub>P<sub>0.65</sub> layer, in which we are able to observe that the intersections in the  $(1\bar{1}0)$  plane of the boundaries between As-rich and P-rich clusters appear to be preferentially oriented along the  $[\bar{1}12]$  and  $[1\bar{1}2]$  directions in the crystal. The dashed lines in the magnified image delineate a single As-rich cluster within the InAs<sub>0.35</sub>P<sub>0.65</sub> alloy. The cluster appears to be approximately triangular in cross-section, with the lower InAs<sub>0.35</sub>P<sub>0.65</sub>/InP interface constituting a base extending approximately  $6\text{--}7$  nm in the  $[\bar{1}10]$  direction; two sides oriented along the  $[\bar{1}12]$  and  $[1\bar{1}2]$  directions form a triangular region approximately  $3.5\text{--}4$  nm in height. If we assume that the boundaries between As-rich and P-rich clusters are simple planes, we may deduce from the intersections of the cluster boundaries with the  $(1\bar{1}0)$  cross-sectional plane that the boundary plane indices  $(hkl)$  should satisfy the equation  $\mp(h-k) + 2l = 0$ , the simplest solutions to which correspond to the  $(\bar{1}11)$  and  $(1\bar{1}1)$  planes in the crystal.

Further information about the nanoscale compositional structure of the InAs<sub>0.35</sub>P<sub>0.65</sub> alloy layers may be obtained by analysis of cross-sectional images of the  $(1\bar{1}0)$  plane. Fig. 7 shows a three-dimensional rendering of a  $40 \times 40$  nm<sup>2</sup>  $(1\bar{1}0)$  cross-sectional constant-current image of the InP/InAs<sub>0.35</sub>P<sub>0.65</sub> heterostructure, obtained at a sample bias of  $-2.4$  V and a tunneling current of  $0.1$  nA. A clear asymmetry in interfacial abruptness consistent with that seen in the  $(110)$  cross-sectional image is also seen for this orientation. In addition, the InAs<sub>0.35</sub>P<sub>0.65</sub> alloy layers show considerably less compositional variation along the  $[1\bar{1}0]$  direction than was evident along the  $[\bar{1}10]$  direction in the  $(110)$  cross-sectional image. The relatively uniform As composition observed along the  $[1\bar{1}0]$  lateral direction in the  $(1\bar{1}0)$  cross-sectional image combined with the

triangular cross-sections of the As-rich and P-rich clusters observed in the  $(110)$  image suggest that As-rich and P-rich clusters in the InAs<sub>0.35</sub>P<sub>0.65</sub> alloy tend to be elongated along the  $[1\bar{1}0]$  direction, with roughly triangular cross-sections in the  $(110)$  plane.

## 5. Conclusions

As illustrated by the studies described in the previous sections, cross-sectional STM has proven to be a powerful technique for probing the properties of advanced semiconductor materials and device structures at the atomic to nanometer scale. The ability to characterize atomic-scale interface, alloy layer, and defect structure in III–V compound semiconductor materials is by now relatively well established, and it is likely that characterization by cross-sectional STM will contribute increasingly to the development and optimization of advanced heterostructure and nanoscale devices in which atomic-scale structure and electronic properties are of paramount importance. To this end, it will be of particular interest to continue to investigate and establish correlations between results of atomic- to nanometer-scale characterization by cross-sectional STM, and information about material and device properties obtained using other measurements that probe different properties, that are sensitive to properties at larger length scales, or are otherwise complementary to cross-sectional STM. Such studies will provide more complete data about the detailed relationship between atomic-scale properties and device behavior, and help confirm that information obtained from high-resolution measurements over a small area or volume, as is obtained in cross-sectional STM, is indeed representative of the whole.

## Acknowledgements

The author would like to acknowledge the contributions of Dr. A.Y. Lew, S.L. Zuo, Dr. R.H. Miles, Dr. W.G. Bi, and Professor C.W. Tu to various aspects of the work described here. Part of this work was supported by the National Science Foundation under Award Nos. ECS 93-07986 and ECS 95-01469, by Hughes Aircraft Company through the University of California MICRO program, by DARPA through the Optoelectronics Technology Center, and by an Alfred P. Sloan Research Fellowship.

## References

- Bhattacharya, P.K., Ku, J.W., 1985. Effect of alloy clustering on the high-temperature electron mobility in  $\text{In}_{1-x}\text{Ga}_x\text{As}_y\text{P}_{1-y}$ . *J. Appl. Phys.* 58, 1410–1411.
- Bimberg, D., Grundmann, M., Ledentsov, N.N., 1998. Growth spectroscopy laser application of self-ordered III–V quantum dots. *MRS Bulletin* 23, 31–34.
- Brar, B., Ibbetson, J., Kroemer, H., English, J.H., 1994. Effects of the

- interface bonding type on the optical and structural properties of InAs-AlSb quantum wells. *Appl. Phys. Lett.* 64, 3392–3394.
- Chow, D.H., Miles, R.H., Hunter, A.T., 1992. Effects of interface stoichiometry on the structural and electronic properties of  $\text{Ga}_{1-x}\text{In}_x\text{Sb}/\text{InAs}$  superlattices. *J. Vac. Sci. Technol. B* 10, 888–891.
- Collins, D.A., Wang, M.W., Grant, R.W., McGill, T.C., 1994. Reflection high energy electron diffraction observation of anion exchange reactions on InAs surfaces. *J. Appl. Phys.* 75, 259–262.
- Dijkkamp, D., Van Loenen, E.J., Hoeven, A.J., Dieleman, J., 1990. Scanning tunneling microscopy study of Si (0 0 1) and Si (1 1 0) surface structures resulting from different thermal cleaning treatments. *J. Vac. Sci. Technol. A* 8, 218–221.
- Feenstra, R.M., Stroscio, J.A., Tersoff, J., Fein, A.P., 1987. Atom-selective imaging of the GaAs (1 1 0) surface. *Phys. Rev. Lett.* 58, 1192–1195.
- Feenstra, R.M., Collins, D.A., Ting, D.Z.-Y., Wang, M.W., McGill, T.C., 1994. Interface roughness and asymmetry in InAs/GaSb superlattices studied by scanning tunneling microscopy. *Phys. Rev. Lett.* 72, 2749–2752.
- Förster, A., Lange, J., Gerthsen, D., Dieker, Ch., Lüth, H., 1993. Effect of interface roughness and scattering on the performance of AlAs/InGaAs resonant tunneling diodes. *J. Vac. Sci. Technol. B* 11, 1743–1747.
- Gomyo, A., Suzuki, T., 1988. Observation of strong ordering in  $\text{Ga}_x\text{In}_{1-x}\text{P}$  alloy semiconductors. *Phys. Rev. Lett.* 60, 2645–2648.
- Goodnick, S.M., Ferry, D.K., Wilmsen, C.W., Liliental, Z., Fathy, D., Krivanek, O.L., 1985. Surface roughness at the Si (1 0 0)– $\text{SiO}_2$  interface. *Phys. Rev. B* 32, 8171–8186.
- Heller, E.J., Lagally, M.G., 1992. In situ scanning tunneling microscopy observation of surface morphology of GaAs (0 0 1) grown by molecular beam epitaxy. *Appl. Phys. Lett.* 60, 2675–2677.
- Hoffman, C.A., Meyer, J.R., Youngdale, E.R., Bartoli, F.J., Miles, R.H., 1993. Interface roughness scattering in semiconducting and semimetallic InAs– $\text{Ga}_{1-x}\text{In}_x\text{Sb}$  superlattices. *Appl. Phys. Lett.* 63, 2210–2212.
- Hoffman, C.A., Meyer, J.R., Youngdale, E.R., Bartoli, F.J., Miles, R.H., Ram-Mohan, L.R., 1994. Electron transport in InAs/ $\text{Ga}_{1-x}\text{In}_x\text{Sb}$  superlattices. *Solid-State Elect.* 37, 1203–1206.
- Hou, H.Q., Cheng, A.N., Wieder, H.H., Chang, W.S.C., Tu, C.W., 1993. Electroabsorption of InAsP–InP strained multiple quantum wells for 1.3  $\mu\text{m}$  waveguide modulators. *Appl. Phys. Lett.* 63, 1833–1835.
- Ihm, Y.-E., Otsuka, N., Klem, J., Morkoç, H., 1987. Ordering in  $\text{GaAs}_{1-x}\text{Sb}_x$  grown by molecular beam epitaxy. *Appl. Phys. Lett.* 51, 2013–2015.
- Jen, H.R., Ma, K.Y., Stringfellow, G.B., 1989. Long-range order in InAsSb. *Appl. Phys. Lett.* 54, 1154–1156.
- Jen, H.R., Cao, D.S., Stringfellow, G.B., 1989. Long-range (1 1 1) ordering in  $\text{GaAs}_{1-x}\text{P}_x$ . *Appl. Phys. Lett.* 54, 1890–1892.
- Johnson, M.B., Halbout, J.-M., 1992. Scanning tunneling microscopy and spectroscopy for studying cross-sectioned Si (1 0 0). *J. Vac. Sci. Technol. B* 10, 508–514.
- Kim, D.S., Forrest, S.R., Olsen, G.H., Lange, M.J., Martinelli, R.U., Di Giuseppe, N.J., 1995. Avalanche gain in  $\text{InAs}_y\text{P}_{1-y}$  ( $0.1 < y < 0.3$ ) photodetectors. *IEEE Photon. Technol. Lett.* 7, 911–913.
- Lew, A.Y., Yu, E.T., Chow, D.H., Miles, R.H., 1994. Scanning tunneling microscopy of InAs/ $\text{Ga}_{1-x}\text{In}_x\text{Sb}$  superlattices. *Appl. Phys. Lett.* 65, 201–203.
- Lew, A.Y., Zuo, S.L., Yu, E.T., Miles, R.H., 1997. Anisotropy and growth-sequence dependence of atomic-scale interface structure in InAs/ $\text{Ga}_{1-x}\text{In}_x\text{Sb}$  superlattices. *Appl. Phys. Lett.* 70, 75–77.
- Lew, A.Y., Zuo, S.L., Yu, E.T., Miles, R.H., 1998. Correlation between atomic-scale structure and mobility anisotropy in InAs/ $\text{Ga}_{1-x}\text{In}_x\text{Sb}$  superlattices. *Phys. Rev. B* 57, 6534–6539.
- Lutz, M.A., Feenstra, R.M., Chu, J.O., 1995. Scanning tunneling microscopy of in situ cleaved and hydrogen passivated Si (1 1 0) cross-sectional surfaces. *Surf. Sci.* 328, 215–226.
- Mäder, K.A., Zunger, A., 1994. Effects of atomic clustering on the optical properties of III–V alloys. *Appl. Phys. Lett.* 64, 2882–2884.
- Miles, R.H., Chow, D.H., Hamilton, W.J., 1992. High structural quality  $\text{Ga}_{1-x}\text{In}_x\text{Sb}/\text{InAs}$  strained-layer superlattices grown on GaSb substrates. *J. Appl. Phys.* 71, 211–214.
- Miles, R.H., Schulman, J.N., Chow, D.H., McGill, T.C., 1993. Electronic band structure of far-infrared  $\text{Ga}_{1-x}\text{In}_x\text{Sb}/\text{InAs}$  superlattices. *Semicond. Sci. Technol.* 8, S102–S105.
- Muralt, P., Pohl, D.W., 1986. Scanning tunneling potentiometry. *Appl. Phys. Lett.* 48, 514–516.
- Pashley, M.D., Haberern, K.W., Gaines, J.M., 1991. Scanning tunneling microscopy comparison of GaAs (0 0 1) vicinal surfaces grown by molecular beam epitaxy. *Appl. Phys. Lett.* 58, 406–408.
- Salemink, H.W.M., Meier, H.P., Ellialtioglu, R., Gerritsen, J.W., Muralt, P.R.M., 1989. Tunnel spectroscopy of the AlGaAs–GaAs heterostructure interface. *Appl. Phys. Lett.* 54, 1112–1114.
- Skala, S.L., Wu, W., Tucker, J.R., Lyding, J.W., Seabaugh, A., Beam, E.A. III, Jovanovic, D., 1995. Interface characterization in an InP/InGaAs resonant tunneling diode by scanning tunneling microscopy. *J. Vac. Sci. Technol. B* 13, 660–663.
- Smith, A.R., Gwo, S., Sadra, K., Shih, Y.C., Streetman, B.G., Shih, C.K., 1994. Comparative study of cross-sectional scanning tunneling microscopy spectroscopy on III–V heterostructures and homostructures – ultrahigh vacuum-cleaved versus sulfide passivated. *J. Vac. Sci. Technol. B* 12, 2610–2615.
- Stringfellow, G.B., Chen, G.S., 1991. Atomic ordering in III/V semiconductor alloys. *J. Vac. Sci. Technol. B* 9, 2182–2188.
- Sudijono, J., Johnson, M.D., Snyder, C.W., Elowitz, M.B., Orr, B.G., 1992. Surface evolution during molecular-beam epitaxy deposition of GaAs. *Phys. Rev. Lett.* 69, 2811–2814.
- Tanaka, M., Noda, T., Sakaki, H., 1992. Atomic-scale characterization and control of semiconductor interfaces grown by molecular beam epitaxy: interface roughness and electronic and optical properties. *Mater. Sci. Eng. B* 14, 304–310.
- Thibado, P.M., Bennett, B.R., Twigg, M. E., Shanabrook, B.V., Whitman, L.J., 1995. Origins of interfacial disorder in GaSb/InAs superlattices. *Appl. Phys. Lett.* 67, 3578–3580.
- Tuttle, G., Kroemer, H., English, J.H., 1990. Effects of interface layer sequencing on the transport properties of InAs/AlSb quantum wells – evidence for antisite donors at the InAs/AlSb interface. *J. Appl. Phys.* 67, 3032–3037.
- Wang, M.W., Collins, D.A., McGill, T.C., Grant, R.W., 1993. X-ray photoelectron spectroscopy investigation of the mixed anion GaSb/InAs interface. *J. Vac. Sci. Technol. B* 11, 1418–1422.
- Woodward, T.K., Chiu, T.-H., Sizer II, T., 1992. Multiple quantum well light modulators for the 1.06  $\mu\text{m}$  range on InP substrates –  $\text{In}_x\text{Ga}_{1-x}\text{As}_y\text{P}_{1-y}/\text{InP}$ ,  $\text{InAs}_y\text{P}_{1-y}/\text{InP}$  and coherently strained  $\text{InAs}_y\text{P}_{1-y}/\text{In}_x\text{Ga}_{1-x}\text{P}$ . *Appl. Phys. Lett.* 6, 2846–2848.
- Van Loenen, E.J., Dijkkamp, D., Hoeven, A.J., 1988. Clean and metal-contaminated Si (1 1 0) surfaces studied by RHEED, XPS and STM. *J. Microscopy* 152, 487–496.
- Zheng, J.F., Walker, J.D., Salmeron, M.B., Weber, E.R., 1994. Interface segregation and clustering in strained-layer InGaAs/GaAs heterostructures studied by cross-sectional scanning tunneling microscopy. *Phys. Rev. Lett.* 72, 2414–2417.